

# Chapter 3

## Cosmological bounds on dark matter-photon coupling

---

In this chapter, we investigate an extension of the  $\Lambda$ CDM model where DM is coupled to photons (we call it DM-photon coupling model), inducing a non-conservation of the numbers of particles for both species, where the DM particles are allowed to dilute throughout the cosmic history with a small deviation from the standard evolution decaying into photons, while the associated scattering processes are assumed to be negligible. In the first study, we investigate DM-photon coupling model by taking a constant DE EoS not equal to minus one and the presence of massive neutrinos with the effective number of neutrino species,  $N_{\text{eff}}$  as a free parameter. In the second study, we extend the first case by considering time-varying DE EoS via CPL parameterization with the motivation to observe the possible effect of variable DE on the coupling model. We analyze the effects of the DM-photon coupling on the CMB and matter power spectra in both studies. Our main aim here is to investigate the observational constraints on both the cosmological scenarios by using the data from the measurements of CMB, BAO, HST, and LSS information from the abundance of galaxy clusters. The research work presented in this chapter is carried out in the research papers [104, 105].

### 3.1 Introduction

The phenomenon of decay of DM into species like dark radiation, photons, neutrinos, etc. has been considered in the literature in different contexts and motivations. A review of decaying DM signals in gamma-rays, cosmic ray antimatter, and neutrinos can be seen in [106]. More intensively, the search for DM decay has been carried out by using the Ice-Cube telescope data [107]. Many theoretical/phenomenological studies have been carried out with DM decay models in order to look for some possible solutions to the problems associated with the standard  $\Lambda$ CDM cosmology. For instance, the evidence for DM-dark radiation interaction is reported in [108] where it has been found that this interaction allows reconciling the  $\sigma_8$  tension between Planck CMB and LSS measurements. It has been observed in [109, 110] that the late-time decay of DM is helpful in reconciling some of the small-scale structure formation problems associated with the standard  $\Lambda$ CDM cosmology. Also, see [111–117], where the interaction between DM and dark radiation has been investigated. The decay of DM into photons (and photons + neutrinos) has been investigated from cosmic-ray emission in [118–120]. An analytical and numerical study of DM-photon interactions has been performed in [121] where some consequences of DM-photon interaction on structure formation have been explored. Recently, the constraints on DM-photon scattering-cross section in the early Universe have been obtained in [122]. The upper bounds on the decay width of DM into different final states can be investigated by searching decaying DM. An upper limit on the DM-photon elastic scattering cross section  $\sigma_{\text{DM}-\gamma} \lesssim 10^{-32} (m_{\text{DM}}/\text{GeV}) \text{ cm}^2$  has been derived in [123]. An upper bound on elastic scattering cross section of DM-neutrino and DM-DE have been obtained as  $\sigma_{\text{DM}-\nu} \lesssim 10^{-33} (m_{\text{DM}}/\text{GeV}) \text{ cm}^2$  and  $\sigma_{\text{DM}-\text{DE}} \lesssim 10^{-29} (m_{\text{DM}}/\text{GeV}) \text{ cm}^2$  in [124] and [125], respectively. Despite the success of the  $\Lambda$ CDM model, where DM particles interact only gravitationally with other particles, some free parameters of this model are currently in tension with some direct and local observational estimates. The well-known tensions are in the estimation of Hubble constant,  $H_0$  and amplitude of matter density fluctuations,  $\sigma_8$  from Planck-CMB data and direct measurements (as discussed

in Chapter 1). However, these tensions may be the outcome of the systematic effects in data rather than a hint of new physics beyond  $\Lambda$ CDM. For instance, the authors in [126] argue that the supernovae measurements of  $H_0$  are overestimated due to the local environment bias in supernovae type Ia standardized magnitudes. On the other hand, the findings in [127] suggest that the tension in  $H_0$  distance ladders is likely not a result of supernova systematics that could be expected to vary between optical and near-infrared wavelengths, like dust extinction. Likewise, the tension on  $\sigma_8$  has at least two sources: i) the galaxy cluster counts; ii) weak lensing. From the side of the galaxy cluster counts, the ways to alleviate  $\sigma_8$  tension have been discussed in [47]. Furthermore, the new results on the weak lensing by the Dark Energy Survey (DES) collaboration [101] exhibit no tension in the  $\sigma_8$ -parameter measurement. The possible systematic effects in the discrepancy between CMB and LSS are also discussed in [46]. Here, we consider a cosmological model with a non-minimal DM-photon coupling in which the interaction is assumed to lead a scenario where the DM decays into photons. This phenomenological scenario of DM-photon coupling can be justified for a possible “dark electromagnetism”, as proposed initially in [128] for DM-dark radiation coupling.

In the next section, we describe the background and perturbation equations of the DM-photon coupling model. In Section 3.3, we discuss the observational constraints on the DM-photon coupling model with constant DE. In Section 3.4, we discuss the observational constraints on the DM-photon coupling model with a time-varying DE. Section 3.5 carries the discussion of model comparison with a reference model. The final Section carries the concluding remarks of this chapter. In what follows, a subindex 0 attached to any parameter means the value of the parameter at the present time. An over dot and prime represent the cosmic time and conformal time derivatives, respectively.

## 3.2 Background and perturbation equations of the model

The background evolution energy density  $\rho_{\text{ddm}}$  of the decaying cold DM follows the standard line already well known in the literature, where a non-conservation of the number density of DM particles leads to non-conservation of the energy-momentum tensor of the

DM particles,  $\nabla_\mu T_{\text{ddm}}^{\nu\mu} = Q$ . Here the coupling function  $Q$  accounts for the decay of DM. The index ddm represents decaying DM. In the present study, we consider that DM can decay into photons. Thus, the background density equations, assuming FLRW Universe, take the form

$$\rho'_{\text{ddm}} + 3\frac{a'}{a}\rho_{\text{ddm}} = -\frac{a'}{a}\Gamma_\gamma\rho_{\text{ddm}}, \quad (3.1)$$

$$\rho'_\gamma + 4\frac{a'}{a}\rho_\gamma = \frac{a'}{a}\Gamma_\gamma\rho_{\text{ddm}}, \quad (3.2)$$

where  $\Gamma_\gamma$  is a dimensionless parameter characterizing the coupling between DM and photons, and prime denotes the conformal time derivative. The quantity  $\rho_\gamma$  is the energy density of photons. It is known that the energy-momentum conservation equation of  $i$ th coupled fluid in a cosmological scenario reads as  $\nabla_\mu T_i^{\nu\mu} = Q_i^\nu$  with  $\sum_i Q_i^\nu = 0$ . We notice that eqs. (3.1) and (3.2) satisfy this condition with  $Q_{\text{ddm}} = -a'/a\Gamma_\gamma\rho_{\text{ddm}}$  and  $Q_\gamma = a'/a\Gamma_\gamma\rho_{\text{ddm}}$ , respectively. We adopt  $\Gamma_\gamma > 0$  in order to have a decaying DM along with the cosmic expansion. Usually, the DM decay rate is considered constant. But in principle, it could be a time variable as well. So without loss of generality, in our model, the decay rate with respect to the proper time can be defined as  $\Gamma = \Gamma_\gamma H$ , where  $H$  is the expansion rate of the Universe. Solving eqs. (3.1) and (3.2), we find

$$\rho_{\text{ddm}} = \rho_{\text{ddm}0}a^{-3-\Gamma_\gamma}, \quad (3.3)$$

$$\rho_\gamma = \rho_{\gamma 0}a^{-4} + \frac{\Gamma_\gamma}{1-\Gamma_\gamma}\rho_{\text{ddm}0}(a^{-3-\Gamma_\gamma} - a^{-4}), \quad (3.4)$$

where for  $\Gamma_\gamma = 0$ , we recover the standard evolution equations for the DM and photons. Now we consider the evolution of linear cosmological perturbations in our model. In the

synchronous gauge, the line element of the linearly perturbed FRW metric is given by

$$ds^2 = -a^2 d\tau^2 + a^2 [(1 - 2\eta)\delta_{ij} + 2\partial_i \partial_j E] dx^i dx^j, \quad (3.5)$$

where  $k^2 E = -2/h - 3\eta$ , restricting to the scalar modes  $h$  and  $\eta$ . Using  $\nabla_\mu T_i^{\nu\mu} = Q_i^\nu$ , the continuity and Euler equations of the  $i$ th coupled fluid, given the above metric, are written as

$$\begin{aligned} \delta'_i + 3H(c_{s,i}^2 - w_i)\delta_i + 9H^2(1 + w_i)(c_{s,i}^2 - c_{a,i}^2)\frac{\theta_i}{k^2} + (1 + w_i)\theta_i - 3(1 + w_i)\eta' \\ + (1 + w_i)\left(\frac{h'}{2} + 3\eta'\right) = \frac{a}{\rho_i}(\delta Q_i - Q_i\delta_i) + a\frac{Q_i}{\rho_i}\left[3H(c_{s,i}^2 - c_{a,i}^2)\right]\frac{\theta_i}{k^2}, \end{aligned} \quad (3.6)$$

$$\theta'_i + H(1 - 3c_{s,i}^2)\theta_i - \frac{c_{s,i}^2}{(1 + w_i)}k^2\delta_i = \frac{aQ_i}{(1 + w_i)\rho_i}\left[\theta_{\text{ddm}} - (1 + c_{s,i}^2)\theta_i\right], \quad (3.7)$$

where we have chosen the momentum transfer in the rest frame of DM. Here,  $w_i$ ,  $c_{a,i}^2$ , and  $c_{s,i}^2$  are the EoS, adiabatic sound speed, and physical sound speed in the rest frame of the  $i$ th fluid, respectively. As expected, for  $Q_i = 0$  in the above equations, we obtain the standard continuity and Euler equations of the  $i$ th fluid. This methodology was initially used to describe the linear perturbations of a dark sector interaction between DM and DE (see [129] and references therein). The next step is to particularize the fluid approximation equations to the coupled system of DM and photon. We have,

$$\delta'_\gamma + \frac{4}{3}\theta_\gamma + \frac{2}{3}h' = a\Gamma_\gamma H\frac{\rho_{\text{ddm}}}{\rho_\gamma}(\delta_{\text{ddm}} - \delta_\gamma), \quad (3.8)$$

$$\theta'_\gamma - \frac{1}{4}k^2(\delta_\gamma - 4\sigma_\gamma) - an_e\sigma_T(\theta_b - \theta_\gamma) = \frac{3}{4}a\Gamma_\gamma H\frac{\rho_{\text{ddm}}}{\rho_\gamma}(\theta_{\text{ddm}} - \frac{4}{3}\theta_\gamma), \quad (3.9)$$

describing the continuity and Euler equations for photons, respectively. Lastly, the DM evolution is given by

$$\delta'_{\text{ddm}} + \frac{h'}{2} = 0. \quad (3.10)$$

In (3.9),  $\theta_b$  is the divergence of baryons fluid velocity, where the term  $an_e\sigma_T(\theta_b - \theta_\gamma)$  is due to the collision term before recombination between photons and baryons, which are tightly coupled, interacting mainly via Thomson scattering. The Euler equation derived for DM in the synchronous gauge reads  $\theta_{\text{ddm}} = 0$ . Recently, the authors in [122] have considered an elastic scattering between DM and photons, and described the complete treatment to Boltzmann hierarchy for photons, including changes in expansion for  $l \geq 3$ . Here, we are considering that the interaction between DM and photons is interpreted for a non-conservation in the numbers of particles for both species, where the DM particles can undergo dilution throughout the cosmic history with a small deviation from the standard evolution decaying into photons. Thus, the process here is different from the DM-photon elastic scattering interaction, where the number of particle density is always conserved, and changes do not occur at background level as well as to continuity equations of the DM and photons. Beyond the changes in the Euler and continuity equations (also in the background dynamics), we believe that a complete treatment of Boltzmann hierarchy for  $l \geq 3$  must also be carried out in our model, but this is beyond our goal in the first steps of the present investigation.

### 3.3 DM-photon coupling with constant dark energy

In general, it is common to consider only the  $\Lambda$ CDM model as a cosmological scenario to investigate decaying DM models. Here, we consider that DE is in the form of a perfect fluid with a constant EoS parameter  $w_{\text{de}0} \neq -1$ , and investigate its possible effects and deviations from the  $\Lambda$ CDM case in the context under study. Also, to the best of our knowledge, the constraints on  $w_{\text{de}0}$  from the cosmological data have not yet been studied in the context of the decaying DM. We have also considered the presence of neutrinos and

Table 3.1: Uniform priors on the parameters of DM-photon coupling model

Parameter	Prior
$100\omega_b$	[1.8, 2.4]
$\omega_{\text{cdm}}$	[0.01, 0.99]
$100\theta_s$	[0.5, 2.5]
$\ln[10^{10}A_s]$	[2.7, 4.0]
$n_s$	[0.9, 1.3]
$\tau_{\text{reio}}$	[0.01, 0.8]
$\sum m_\nu$	[0.06, 1.0]
$N_{\text{eff}}$	[1.0, 4.0]
$\Gamma_\gamma$	[0, 0.0001]

set the order of mass on the normal hierarchy with a minimum sum of neutrino mass to be 0.06 eV. The total effective number of relativistic species ( $N_{\text{eff}}$ ) is also taken as a free parameter. Therefore, the parametric space for the DM-photon coupling with a constant DE is given below

$$P = \{\omega_b, \omega_{\text{cdm}}, \theta_s, A_s, n_s, \tau_{\text{reio}}, w_{\text{de}0}, \sum m_\nu, N_{\text{eff}}, \Gamma_\gamma\},$$

where the first six parameters are the base parameters of  $\Lambda$ CDM model, and the rest four are extended parameters. We use the uniform (flat) prior on all model parameters as displayed in Table 3.1

To constrain these free model parameters, we use the data sets from CMB, BAO, HST, and LSS in following four combinations: CMB + BAO, CMB + BAO + LSS, CMB + BAO + HST and CMB + BAO + LSS + HST. Here, LSS data include the measurements from Planck-SZ, CFHTLenS, and KiDS-450. We have chosen CMB + BAO as minimal data set because adding BAO data to CMB reduces the error-bars on the parameters. The other data set combinations are considered in order to investigate how the constraints on various free parameters and derived parameters of the DM-photon coupling model are affected by the inclusion of HST and LSS data.

### 3.3.1 Effects CMB temperature (TT) and matter power spectra

It is well known that a non-conservation in the photon's number density can affect the anisotropy of the CMB. Photon production (or destruction) has been considered in other contexts [130–137]. In general, a change in the standard dynamics of photons can affect CMB and another important cosmological relationship in various ways, like the CMB spectral distortions, secondary CMB anisotropies, luminosity distance, etc. Here, we focus on the background and perturbative changes (as described in this section) in order to test a cosmological scenario with the decay of DM into photons. Figures 3.1 and 3.2 show the theoretical predictions of the CMB TT and matter power spectra at present, i.e., at redshift  $z = 0$ , as well as the relative deviations from the base line Planck 2015  $\Lambda$ CDM model, for the coupling parameter in the range  $\Gamma_\gamma \in [10^{-5}, 10^{-7}]$ . We see that on large angular scales ( $l < 30$ ) we have deviations approximately until 5% and up to 12% on small scales on CMB TT. These changes are quantified by the reduction in magnitude of the acoustic peaks at small scales by collisional damping and the enhancement of the first acoustic peaks due to a decrease in the photons diffusion length. The effects on matter power spectrum are about 10%-15% on large scale and oscillations around 15%-25% on small scale (where nonlinear effects may be predominant). These changes on CMB TT and matter power spectra are similar in order of magnitude or even smaller than in other decaying DM models described in the literature.

### 3.3.2 Results and discussion

Table 3.2 summarizes the observational constraints on the free parameters and some derived parameters of the DM-photon coupling model for the four combinations of data sets: CMB + BAO, CMB + BAO + LSS, CMB + BAO + HST and CMB + BAO + LSS + HST.

We note that with all the data sets analyzed here, the DM-photon coupling parameter  $\Gamma_\gamma$  is very small with the order  $10^{-5}$ . The 95% limits are displayed in Table 3.2,

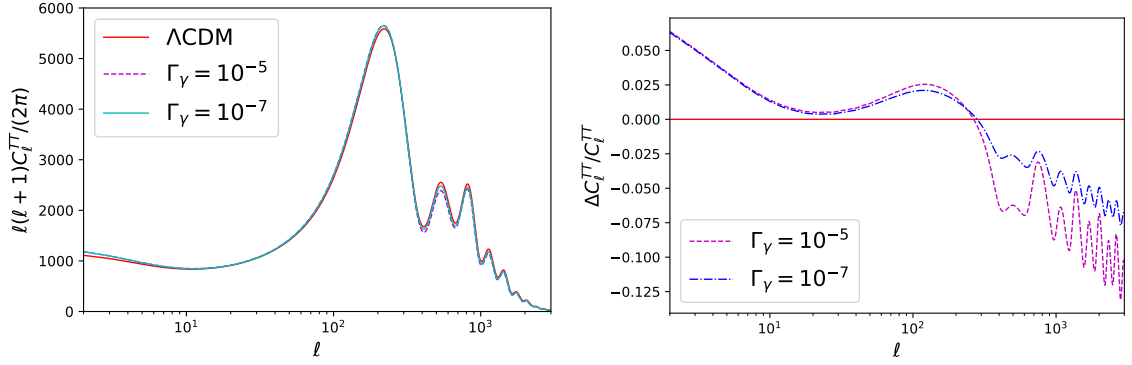


Figure 3.1: Theoretical prediction and relative deviations of the CMB TT power spectrum from the base line Planck 2015  $\Lambda$ CDM model for some values of  $\Gamma_\gamma$  while the other parameters are fixed to their best-fit mean values as given in Table 3.2.

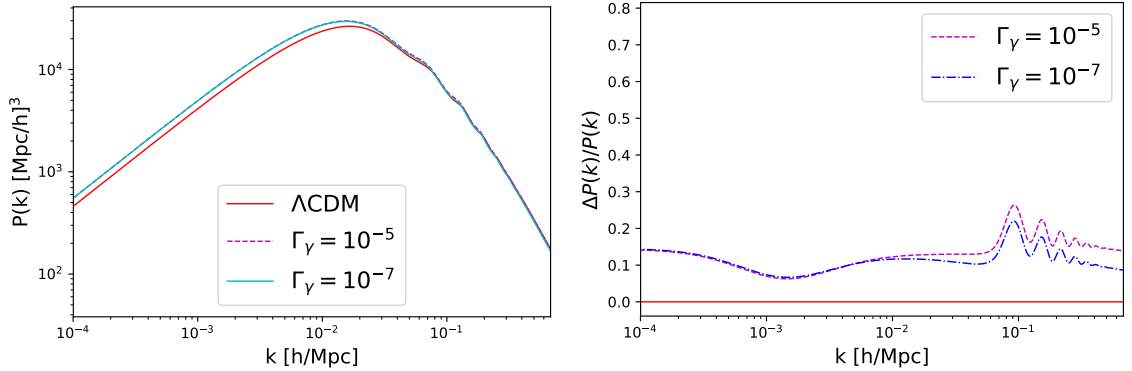


Figure 3.2: Theoretical prediction and relative deviations of the matter power spectrum from the base line Planck 2015  $\Lambda$ CDM model for some values of  $\Gamma_\gamma$  while the other parameters are fixed to their best-fit mean values as given in Table 3.2.

and we have  $\Gamma_\gamma \leq 1.3 \times 10^{-5}$  from the joint analysis using full data CMB + BAO + LSS + HST. Also, see Figure 3.3 that shows the one-dimensional marginalized distribution for  $\Gamma_\gamma$ . The coupling parameter has the same order of magnitude in all four cases, but a smaller amplitude is observed in the case CMB + BAO + HST. Even though it is too small (reasonably expected), the non-conservation of photons due to the DM-photon coupling leads to significant effects on the CMB, which can directly affect the other cosmological parameters, in particular,  $H_0$  and  $\sigma_8$ . Further, the constraints on  $w_{\text{de}0}$  with CMB + BAO + LSS and full data CMB + BAO + LSS + HST are  $w_{\text{de}0} = -1.15^{+0.12}_{-0.10}$  and  $w_{\text{de}0} = -1.13^{+0.11}_{-0.09}$  both at 68% CL, respectively. Therefore, a phantom behaviour of

Table 3.2: Constraints on the free parameters and some derived parameters of the DM-photon coupling model for four combinations of data sets. The upper and lower values with the mean value of each parameter denote 68% CL and 95% CL errors. For  $\sum m_\nu$  and  $\Gamma_\gamma$ , the upper bounds at 95% CL are mentioned. The parameter  $H_0$  is measured in the units of  $\text{km s}^{-1} \text{Mpc}^{-1}$ ,  $r_{\text{drag}}$  in Mpc, whereas  $\sum m_\nu$  is in the units of eV. The  $\chi^2_{\text{min}}$  values of the fit are also shown in last row.

Parameter	CMB + BAO	CMB + BAO + LSS	CMB + BAO + HST	CMB + BAO + LSS + HST
$10^2 \omega_b$	$2.29^{+0.14+0.27}_{-0.14-0.26}$	$2.34^{+0.19+0.31}_{-0.16-0.34}$	$2.33^{+0.09+0.19}_{-0.09-0.18}$	$2.31^{+0.09+0.20}_{-0.09-0.18}$
$\omega_{\text{cdm}}$	$0.127^{+0.013+0.024}_{-0.013-0.025}$	$0.129^{+0.018+0.028}_{-0.015-0.030}$	$0.130^{+0.007+0.016}_{-0.008-0.015}$	$0.125^{+0.007+0.017}_{-0.008-0.015}$
$\ln 10^{10} A_s$	$3.107^{+0.034+0.082}_{-0.045-0.075}$	$3.127^{+0.045+0.087}_{-0.045-0.084}$	$3.108^{+0.038+0.080}_{-0.045-0.077}$	$3.130^{+0.043+0.085}_{-0.043-0.084}$
$100\theta_s$	$1.0412^{+0.0009+0.0021}_{-0.0011-0.0019}$	$1.0409^{+0.0009+0.0023}_{-0.0014-0.0019}$	$1.0409^{+0.0007+0.0015}_{-0.0007-0.0014}$	$1.0411^{+0.0007+0.0016}_{-0.0007-0.0015}$
$n_s$	$0.977^{+0.012+0.028}_{-0.013-0.024}$	$0.978^{+0.013+0.025}_{-0.013-0.024}$	$0.977^{+0.013+0.026}_{-0.013-0.024}$	$0.980^{+0.012+0.025}_{-0.012-0.024}$
$\tau_{\text{reio}}$	$0.084^{+0.017+0.038}_{-0.021-0.036}$	$0.096^{+0.019+0.041}_{-0.022-0.038}$	$0.084^{+0.018+0.038}_{-0.021-0.037}$	$0.098^{+0.020+0.040}_{-0.020-0.039}$
$w_{\text{de0}}$	$-1.03^{+0.10+0.18}_{-0.08-0.19}$	$-1.15^{+0.12+0.20}_{-0.10-0.22}$	$-1.03^{+0.11+0.18}_{-0.08-0.20}$	$-1.13^{+0.11+0.19}_{-0.09-0.20}$
$\sum m_\nu$	$< 0.38$	$< 0.97$	$< 0.37$	$< 0.83$
$N_{\text{eff}}$	$3.51^{+0.43+0.82}_{-0.43-0.84}$	$3.65^{+0.61+0.90}_{-0.46-1.00}$	$3.60^{+0.34+0.69}_{-0.34-0.63}$	$3.58^{+0.36+0.72}_{-0.36-0.68}$
$\Gamma_\gamma$	$< 2.3 \times 10^{-5}$	$< 2.6 \times 10^{-5}$	$< 9.0 \times 10^{-6}$	$< 1.3 \times 10^{-5}$
$\Omega_m$	$0.293^{+0.013+0.026}_{-0.013-0.026}$	$0.284^{+0.015+0.028}_{-0.015-0.029}$	$0.293^{+0.013+0.025}_{-0.013-0.024}$	$0.287^{+0.013+0.025}_{-0.013-0.026}$
$H_0$	$71.9^{+4.0+7.8}_{-4.0-7.1}$	$74.7^{+5.1+10.0}_{-5.1-10.0}$	$72.8^{+1.7+3.2}_{-1.7-3.3}$	$73.3^{+1.7+3.5}_{-1.7-3.3}$
$\sigma_8$	$0.829^{+0.020+0.040}_{-0.020-0.038}$	$0.781^{+0.015+0.028}_{-0.015-0.028}$	$0.829^{+0.019+0.037}_{-0.019-0.037}$	$0.778^{+0.014+0.027}_{-0.014-0.027}$
$r_{\text{drag}}$	$142.5^{+6.8+15}_{-8.2-13}$	$140.5^{+6.1+20.0}_{-11.0-10.0}$	$140.5^{+4.4+8.6}_{-4.4-8.5}$	$141.9^{+4.7+9.4}_{-4.7-9.1}$
$\chi^2_{\text{min}}/2$	5642.11	5650.41	5642.53	5650.58

DE is minimally favored in the DM-photon coupling model when LSS data are included in the analysis. In the other two cases without LSS data, the DE behavior is similar to the cosmological constant since  $w_{\text{de0}} \sim -1$ . See the Figure 3.4, where the vertical line represents  $w_{\text{de0}} = -1$ , cosmological constant.

The interaction between DM and photons gives rise to a very weak ‘‘DM drag’’ which damps the growth of matter density perturbations throughout radiation domination, and therefore can act to reconcile the tension on  $H_0$  between predictions from the CMB and direct measurements. Similar scenario also arises in DM-dark radiation interaction models. Figure 3.5 shows the parametric space of  $H_0 - \sigma_8$ , where the horizontal yellow band corresponds to  $H_0 = 73.24 \pm 1.74 \text{ km s}^{-1} \text{Mpc}^{-1}$ . From Table 3.2, we note that without using any prior on  $H_0$ , we have  $H_0 = 71.9 \pm 4 \text{ km s}^{-1} \text{Mpc}^{-1}$  and  $H_0 = 74.7 \pm 5 \text{ km s}^{-1} \text{Mpc}^{-1}$  both at 68% CL from CMB + BAO and CMB + BAO + LSS, respectively. With

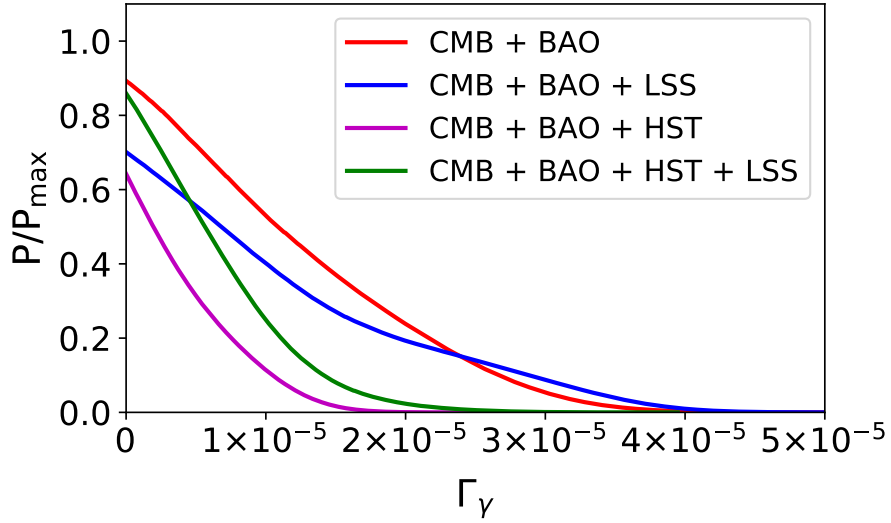


Figure 3.3: One-dimensional marginalized distribution for the coupling parameter  $\Gamma_\gamma$ .

the introduction of HST in the analysis, we have  $H_0 = 72.8 \pm 1.7 \text{ km s}^{-1} \text{ Mpc}^{-1}$  and  $H_0 = 73.3 \pm 1.7 \text{ km s}^{-1} \text{ Mpc}^{-1}$  both at 68% CL from CMB + BAO + HST and joint analysis using full data. Therefore, with all the data sets (with or without using the local prior on  $H_0$ ) the DM-photon coupling model favors the local measurement  $H_0 = 73.24 \pm 1.74 \text{ km s}^{-1} \text{ Mpc}^{-1}$ . Thus, the DM-photon coupling model developed here can serve as an alternative to explain the well-known tension of  $H_0$ . Other perspectives in order to alleviate the tension on  $H_0$  are investigated in [49–52, 138–145]. From Table 3.2, we note that the constraints on  $\sigma_8$  from CMB + BAO + LSS and joint analysis using the full data are  $\sigma_8 = 0.781 \pm 0.028$  and  $\sigma_8 = 0.778 \pm 0.027$ , both at 95% CL, respectively. These, in addition to the common region of the contours in the LSS cases with the vertical light red band in Figure 3.5, indicate some consistency of the DM-photon coupling model based  $\sigma_8$  values with the local measurements like SZ cluster abundances measurements, galaxy cluster count and weak gravitational lensing, etc. Thus, the DM-photon coupling model alleviates the  $\sigma_8$  tension as well to some extent when LSS data is included in the analysis. The upper bound on mass scale of active neutrinos is obtained as  $\sum m_\nu < 0.38 \text{ eV}$  with minimal data set CMB + BAO, whereas a higher upper bound  $\sum m_\nu < 0.83 \text{ eV}$  is obtained with the full data set, both at 95% CL. We see that the constraint on  $\sum m_\nu$

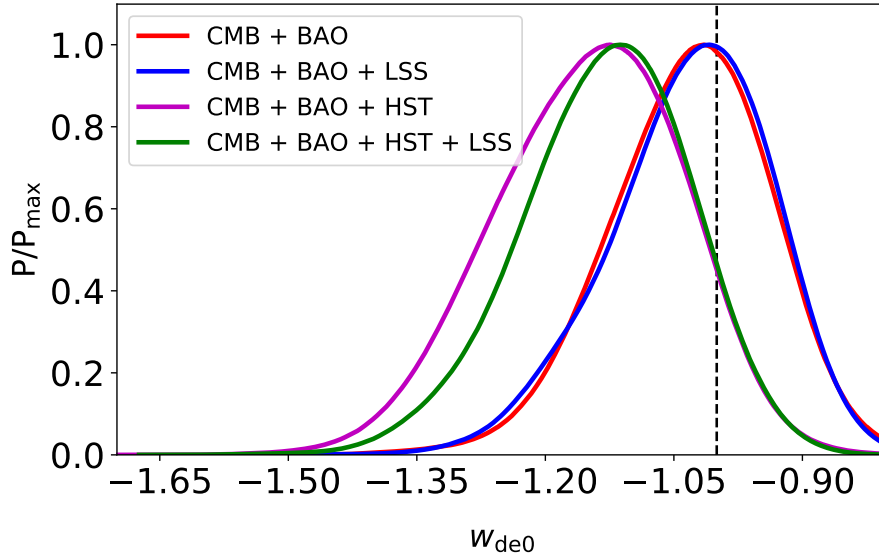


Figure 3.4: One-dimensional marginalized distribution of the present DE EoS parameter,  $w_{\text{de}0}$ . The dashed vertical line corresponds to  $w_{\text{de}0} = -1$ , cosmological constant.

becomes weaker by a factor of two in the case of the full data set. The presence of massive neutrinos reduces the growth of perturbations (reducing the growth rate of structures) below their free-streaming length. Thus, the data from LSS (prior in the  $\sigma_8 - \Omega_m$  plane) which are physically dependent on small scales approximation, and where massive neutrinos play an important role, are responsible for this degeneracy (double the neutrino mass scale in our analysis). It is difficult to quantify the individual physical effects responsible for the constraints on  $\sum m_\nu$ , knowing that many systematic effects (calibration of the mass-observable relation, modeling the number of halos, etc.) can affect LSS data. But, evidently the constraints  $\sum m_\nu < 0.97$  eV and  $\sum m_\nu < 0.83$  eV when LSS data are added in the analysis, are related to the tension on  $\sigma_8$ . These constraints differ up to  $2\sigma$  CL from the ones obtained using CMB + BAO and CMB + BAO + HST data. This difference of about  $2\sigma$  CL is also transmitted to the neutrinos mass scale. Further, we notice that the spectrum index ( $n_s$ ) of the primordial scalar perturbations is compatible with a scale invariant spectrum ( $n_s = 1$ ) at  $2\sigma$  CL in all the four cases of our analysis here. In the case CMB + BAO + LSS + HST,  $n_s = 1$  is compatible at  $1.5\sigma$  CL. Taking the minimal  $\Lambda$ CDM model, Planck team [32] has ruled out  $n_s = 1$  at  $5.6\sigma$  CL. Therefore, the

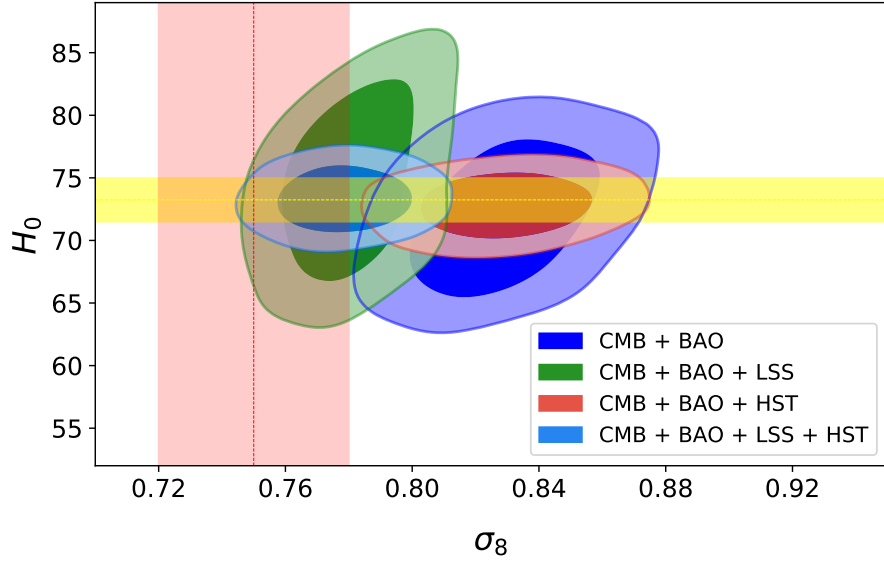


Figure 3.5: Confidence contour (68% and 95% CL) for  $\sigma_8 - H_0$  plane. The horizontal yellow band corresponds to  $H_0 = 73.24 \pm 1.74 \text{ km s}^{-1} \text{ Mpc}^{-1}$  whereas the vertical light red band corresponds to  $\sigma_8 = 0.75 \pm 0.03$ .

extended model presented here (DM-photon coupling +  $N_{\text{eff}}$ ) can reduce it up to  $4\sigma$  CL. Effects of some extended scenarios on  $n_s$  are also discussed in [146]. A scale invariant spectrum is investigated in the light of  $H_0$  and  $\sigma_8$  tensions in [140]. The decay process of DM into photons represents a direct non-conservation in total radiation energy density throughout cosmic history. Thus, it is also expected that this process can also change  $N_{\text{eff}}$  and  $r_{\text{drag}}$  (BAO acoustic scale at drag epoch). These quantities directly depend on  $\rho_\gamma$ . For, the effective number of species can be parametrized (when the neutrinos are relativistic) by

$$N_{\text{eff}} = \frac{8}{7} \left( \frac{4}{11} \right)^{-\frac{4}{3}} \left( \frac{\rho_\nu}{\rho_\gamma} \right). \quad (3.11)$$

As we have a change over  $\rho_\gamma$  from the standard evolution prediction, the non-conservation on photons density can influence  $N_{\text{eff}}$  to non-standard values. Also, a DM-photon coupling can affect the BAO acoustic scale at drag epoch  $r_{\text{drag}}$ , since this quantity depends

tightly on the baryon-photon ratio  $R = 3\rho_b/4\rho_\gamma$ ,

$$r_{\text{drag}}(z_{\text{drag}}) = \int_{z_{\text{drag}}}^{\infty} \frac{c_s(z)}{H(z)} dz, \quad \text{with } c_s(z) = \frac{c}{\sqrt{3 + 3R(z)}}, \quad (3.12)$$

where  $\rho_b$  stands for the baryon density and  $c_s$  is the sound velocity as a function of the redshift. Besides the non-conservation of the photons induced by  $\Gamma_\gamma$ , the addition of  $w_{\text{de}0}$  and  $N_{\text{eff}}$  is expected to cause variations on  $r_{\text{drag}}$  too. The Planck team [32] has reported  $r_{\text{drag}} = 147.60 \pm 0.43$  Mpc from TT + lowP + lensing in the minimal base  $\Lambda$ CDM model. The authors in [147] within  $\Lambda$ CDM +  $N_{\text{eff}}$  have obtained  $r_{\text{drag}} = 143.53 \pm 3.3$  Mpc. Using only low-redshift standard ruler, the constraint  $r_{\text{drag}} = 143.9 \pm 1.9$  Mpc is obtained in [148]. As already mentioned, the three free parameters ( $\Gamma_\gamma$ ,  $w_{\text{de}0}$  and  $N_{\text{eff}}$ ) in our model can affect  $r_{\text{drag}}$ . Figure 3.6 shows the one-dimensional marginalized distribution on  $N_{\text{eff}}$  and  $r_{\text{drag}}$  (measured in Mpc) from the four data combinations used in this work. We find  $r_{\text{drag}} = 142.5^{+6.8}_{-8.2}$  Mpc at 68% CL from CMB + BAO. This value is compatible with all the measures mentioned above at 68% CL. The other values, from the other combinations, are also compatible to the values presented in [32, 147, 148] at 68% CL. But, due to our extended model and the used data combinations, the most reasonable comparison on  $r_{\text{drag}}$  is made for CMB + BAO only. Within our model and analysis, we find that the best fit for  $N_{\text{eff}}$  can deviate significantly from its standard value ( $N_{\text{eff}} = 3.046$ ) in all the cases analyzed here, but when the borders are observed even at 68% CL, no evidence for dark radiation is found. In general, the DM-photon coupling can significantly change the best fit on  $N_{\text{eff}}$  and  $r_{\text{drag}}$ , due to non-conservation of photons through the expansion of the Universe, but the observational bounds are compatible at 68% CL with the standard results of the  $\Lambda$ CDM model.

### 3.4 DM-photon model with time-varying dark energy

This section presents the results on cosmological parameters of the DM-photon coupling model with a time-varying DE EoS via CPL parametrization. The main aim of this extended study is to investigate how a time-varying DE effects the parameters of DM-photon

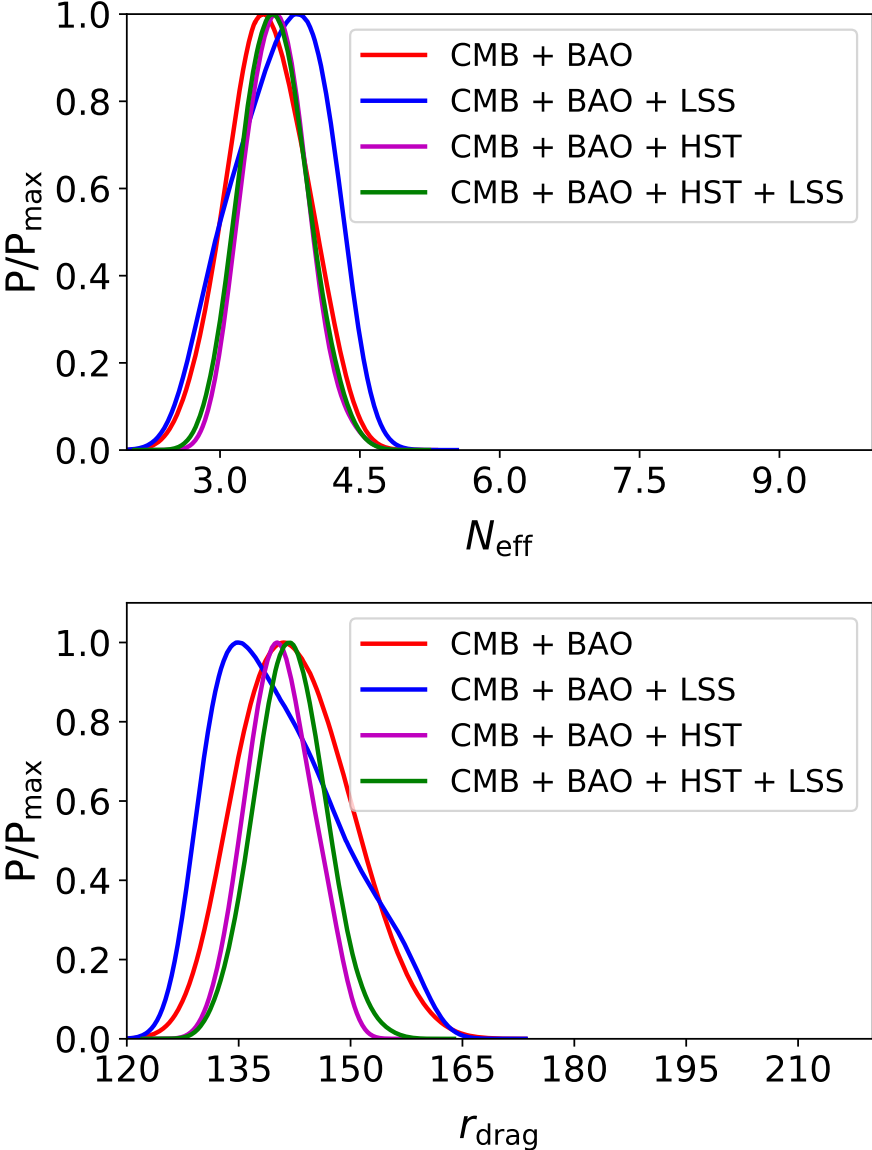


Figure 3.6: One-dimensional marginalized distributions of  $N_{\text{eff}}$  and  $r_{\text{drag}}$ , both are measured in units of Mpc.

coupling. The CPL parametrization for DE [149–152] is an important and widely used parametrization which contains first two terms of the Taylor’s series expansion of EoS about the present scale factor (i.e.,  $a(t)=1$ ) of the Universe. This parametrization for DE is given as

$$w_{\text{de}}(a) = w_{\text{de}0} + w_{\text{de}1}(1 - a), \quad (3.13)$$

where  $w_{\text{de}0}$  and  $w_{\text{de}1}$  are free parameters (constants) to be constrained by the observational data used in the analysis. The parametric space for this extended scenario is

$$\mathcal{P} = \{\omega_{\text{b}}, \omega_{\text{cdm}}, \theta_s, A_s, n_s, \tau_{\text{reio}}, w_{\text{de}0}, w_{\text{de}1}, \sum m_{\nu}, N_{\text{eff}}, \Gamma_{\gamma}\},$$

where as usual the first six parameters are the base parameters of standard model, and remaining are the extended parameters of model under investigation. In this case, we use the same prior on all model parameters as shown in Table 3.1. We choose the range for additional DE EoS parameters:  $w_{\text{de}0} \in [-2.0, 0.5]$  and  $w_{\text{de}1} \in [-1.5, 1.5]$ . For the sake of consistency, in this case we use the same set of data combinations for constraining the free model parameters.

### 3.4.1 Effects on matter and CMB TT power spectra

As discussed in our first model, the matter power spectrum, CMB anisotropies, CMB spectral distortions, luminosity distance etc. can be affected in various ways due to the non-conservation of the photon number density resulting from the decay of DM into photons. Figures 3.7 and 3.8 respectively show the matter and CMB TT power spectra with their relative deviations from standard  $\Lambda$ CDM model for some values of the parameters  $\Gamma_{\gamma}$ ,  $w_{\text{de}0}$ , and  $w_{\text{de}1}$ , as mentioned in legends whereas the other related parameters are kept to their respective mean value from Table 3.3. We notice that the two spectra deviate considerably from the  $\Lambda$ CDM model due to change in  $\Gamma_{\gamma}$  as we observed in our first study. On the other hand, no deviations are observed due to change in the EoS parameters of DE. Thus, the time-varying DE does not affect the matter and CMB power spectra on the top

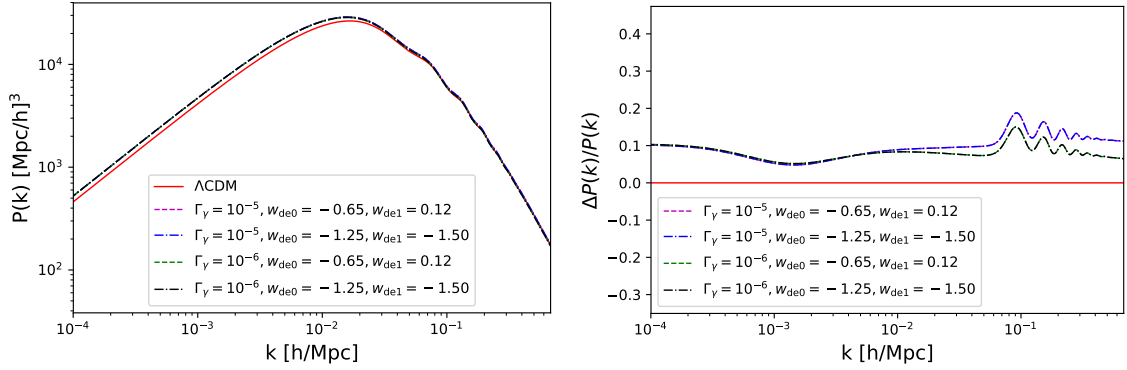


Figure 3.7: The matter power spectrum and its relative deviations from the baseline Planck-2015 standard  $\Lambda$ CDM model for some values of  $\Gamma_\gamma$ ,  $w_{de0}$ , and  $w_{de1}$  mentioned in legend whereas the other related parameters are kept to their respective mean value from Table 3.3.

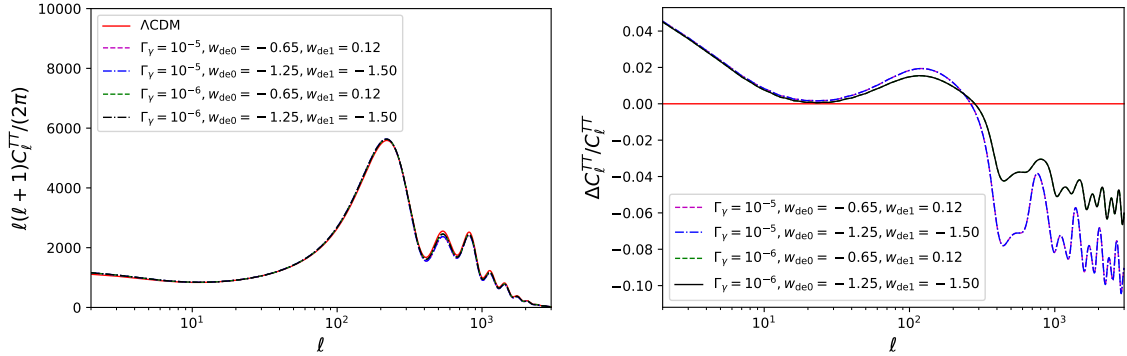


Figure 3.8: The CMB TT power spectrum and its relative deviations from baseline Planck-2015 standard  $\Lambda$ CDM model for some values of  $\Gamma_\gamma$ ,  $w_{de0}$ , and  $w_{de1}$  mentioned in legend whereas the other related parameters are kept to their respective mean value from Table 3.3.

of the DM-photon coupling scenario. In any general modification of  $\Lambda$ CDM cosmology (within DE models), it is expected that the main effects of CMB anisotropies occur on the amplitude of the late time integrated Sachs-Wolfe (ISW) effect, manifested at large angular scales. This effect depends on the duration of the DE domination, i.e., on the time of equality of matter and DE density. So, different behaviors of  $w(z)$  (in this case from CPL model), quintessence or phantom behavior must have opposite effects in  $l < 100$ . So, the values of  $w_{de0}$  and  $w_{de1}$  can be fixed in such a way that DE will show quintessence or phantom behavior at the late time (for instance, for  $z < 2$ ). The constraints on total matter

density ( $\Omega_m$ ) control the amplitude of peaks, especially the second and third peaks. It can be seen from Table 3.3, that the changes on  $\Omega_m$  are minimal, so the amplitude corrections will also be minimal. Also, changes in the expansion of the Universe, at late time from CPL free parameters and early times from  $\Gamma_\gamma$  will contribute to the corrections on the amplitude of all peaks and shifts on the spectrum due to the modification in the angular diameter distance at decoupling (depend on the expansion history of the DM-photon interaction model after decoupling). The magnitudes of corrections are proportional to the possible deviations from the values,  $\Gamma_\gamma = 0$ ,  $w_{\text{de}0} = -1$ , and  $w_{\text{de}1} = 0$ , compared with minimal  $\Lambda$ CDM model. Note that in our work,  $\Gamma_\gamma \ll 1$ . The coupling parameter  $\Gamma_\gamma$  will contribute at small scales because it changes the density of photons at  $z \gg 1$ .

### 3.4.2 Results and discussion

The observational constraints on baseline parameters and some derived parameters of the underlying model are shown in Table 3.3 with four data combinations: CMB + BAO, CMB + BAO + HST, CMB + BAO + LSS and CMB + BAO + HST + LSS (joint analysis). The first six parameters are well consistent with the standard  $\Lambda$ CDM cosmology. With all data combinations, the mean values of  $w_{\text{de}0}$  indicate quintessence behaviour ( $w_{\text{de}0} > -1$ ) of DE. See the one-dimensional marginalized distribution of  $w_{\text{de}0}$  in left panel of Figure 3.9, where the vertical dotted line corresponds to  $w_{\text{de}0} = -1$  (EoS of the DE given by cosmological constant). On the other hand, in our first case with constant EoS of DE, the mean values of  $w_{\text{de}0}$  were in the phantom region ( $w_{\text{de}0} < -1$ ) with all data combinations. The DM-photon coupling parameter  $\Gamma_\gamma$  is approximate of the order  $10^{-5}$  (upper bound at 95% CL) with all data combinations under consideration (see the one-dimensional marginalized distribution of  $\Gamma_\gamma$  in the right panel of Figure 3.9). These constraints on  $\Gamma_\gamma$  are similar to those obtained in our first study where constant EoS of DE was assumed. Thus, the time-varying EoS of DE does not have any significant effect on the DM-photon coupling parameter  $\Gamma_\gamma$ .

Next, we discuss the impact of the time-varying EoS of DE on  $H_0$  and  $\sigma_8$  in the context of the well-known tensions on these parameters within the  $\Lambda$ CDM model. In Figure

Table 3.3: Constraints (68% and 95% CL) on the free parameters and some derived model parameters with four different data combinations are displayed. The parameters  $H_0$  and  $\sum m_\nu$  are measured in the units of  $\text{km s}^{-1} \text{Mpc}^{-1}$  and eV, respectively. The  $\chi^2_{\min}$  values of the fit are also shown in last row.

Parameter	CMB + BAO	CMB + BAO + HST	CMB + BAO + LSS	CMB + BAO + HST + LSS
$10^2 \omega_b$	$2.22^{+0.15+0.19}_{-0.08-0.22}$	$2.32^{+0.08+0.08}_{-0.03-0.12}$	$2.25^{+0.14+0.16}_{-0.06-0.21}$	$2.31^{+0.08+0.09}_{-0.03-0.13}$
$\omega_{\text{cdm}}$	$0.121^{+0.013+0.019}_{-0.009-0.021}$	$0.131^{+0.007+0.013}_{-0.006-0.014}$	$0.121^{+0.012+0.018}_{-0.008-0.021}$	$0.127^{+0.007+0.011}_{-0.006-0.013}$
$100\theta_s$	$1.0415^{+0.0009+0.0020}_{-0.0010-0.0018}$	$1.0407^{+0.0007+0.0014}_{-0.0007-0.0013}$	$1.0414^{+0.0008+0.0021}_{-0.0010-0.0018}$	$1.0409^{+0.0007+0.0014}_{-0.0007-0.0014}$
$\ln 10^{10} A_s$	$3.095^{+0.037+0.079}_{-0.043-0.074}$	$3.102^{+0.039+0.079}_{-0.039-0.076}$	$3.115^{+0.043+0.083}_{-0.043-0.082}$	$3.112^{+0.042+0.085}_{-0.042-0.085}$
$n_s$	$0.974^{+0.013+0.025}_{-0.013-0.024}$	$0.975^{+0.012+0.024}_{-0.012-0.024}$	$0.976^{+0.012+0.025}_{-0.013-0.023}$	$0.977^{+0.012+0.026}_{-0.013-0.023}$
$\tau_{\text{reio}}$	$0.080^{+0.017+0.038}_{-0.020-0.035}$	$0.080^{+0.019+0.038}_{-0.019-0.038}$	$0.092^{+0.019+0.038}_{-0.019-0.038}$	$0.092^{+0.020+0.040}_{-0.020-0.036}$
$w_{\text{de}0}$	$-0.76^{+0.24+0.37}_{-0.16-0.43}$	$-0.89^{+0.18+0.32}_{-0.16-0.33}$	$-0.86^{+0.24+0.38}_{-0.16-0.43}$	$-0.93^{+0.19+0.30}_{-0.14-0.33}$
$w_{\text{de}1}$	$-0.85^{+0.22+1.00}_{-0.62-0.68}$	$-0.62^{+0.42+0.98}_{-0.59-0.88}$	$-0.88^{+0.18+0.96}_{-0.61-0.66}$	$-0.80^{+0.26+0.92}_{-0.65-0.72}$
$\sum m_\nu [95\% \text{ CL}]$	$< 0.39$	$< 0.52$	$< 0.86$	$< 0.89$
$N_{\text{eff}}$	$3.29^{+0.39+0.77}_{-0.39-0.81}$	$3.60^{+0.32+0.65}_{-0.32-0.61}$	$3.40^{+0.43+0.85}_{-0.43-0.89}$	$3.62^{+0.34+0.68}_{-0.34-0.65}$
$\Gamma_\gamma [95\% \text{ CL}]$	$< 2.7 \times 10^{-5}$	$< 5.1 \times 10^{-6}$	$< 2.2 \times 10^{-5}$	$< 7.7 \times 10^{-6}$
$\Omega_m$	$0.320^{+0.023+0.043}_{-0.023-0.045}$	$0.302^{+0.016+0.031}_{-0.016-0.030}$	$0.308^{+0.024+0.043}_{-0.021-0.046}$	$0.299^{+0.016+0.031}_{-0.016-0.031}$
$H_0$	$67.4^{+3.9+8.0}_{-3.9-8.0}$	$72.2^{+1.6+3.2}_{-1.6-3.0}$	$69.8^{+4.1+8.0}_{-4.1-8.0}$	$72.5^{+1.5+2.9}_{-1.5-2.9}$
$\sigma_8$	$0.799^{+0.020+0.052}_{-0.026-0.045}$	$0.816^{+0.022+0.042}_{-0.020-0.047}$	$0.761^{+0.017+0.040}_{-0.021-0.037}$	$0.767^{+0.014+0.031}_{-0.016-0.028}$
$r_{\text{drag}}$	$146.4^{+4.8+13}_{-7.9-11}$	$140.3^{+2.9+7.5}_{-4.1-6.1}$	$144.8^{+4.5+14.0}_{-7.5-11.0}$	$141.0^{+2.8+7.6}_{-4.3-6.3}$
$\chi^2_{\min}/2$	5640.95	5641.80	5648.78	5649.02

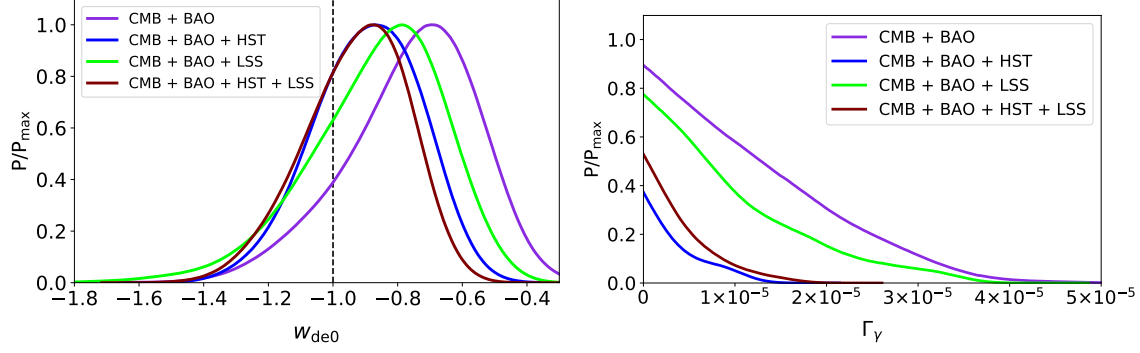


Figure 3.9: One-dimensional marginalized distributions of present DE EoS  $w_{\text{de}0}$  (left panel) and the coupling parameter  $\Gamma_\gamma$  (right panel). The dashed vertical line in the left panel corresponds to  $w_{\text{de}0} = -1$ , cosmological constant.

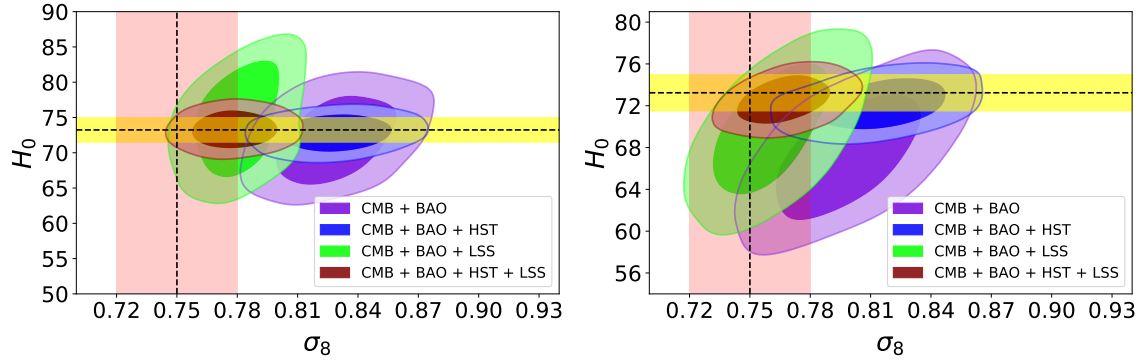


Figure 3.10: 68% and 95% confidence contours for  $H_0$  and  $\sigma_8$  in our first study (left panel) and in present study (right panel). In both panels, the horizontal yellow band shows local value  $H_0 = 73.24 \pm 1.74 \text{ km s}^{-1} \text{ Mpc}^{-1}$  whereas the vertical light red band represents the Planck-SZ measurement:  $\sigma_8 = 0.75 \pm 0.03$ .

3.10, we have shown the parametric space of  $H_0 - \sigma_8$  obtained in our first study (left panel) in contrast with the present study (right panel), where the horizontal yellow band shows local value  $H_0 = 73.24 \pm 1.74 \text{ km s}^{-1} \text{ Mpc}^{-1}$ , reported by Riess *et al.* [39] whereas the vertical light red band represents the Planck-SZ measurement:  $\sigma_8 = 0.75 \pm 0.03$  [43]. We notice clear deviations in the probability regions of the  $H_0$  and  $\sigma_8$  parameters resulting due to the inception of time-varying DE in the present study. These deviations are useful to alleviate the  $H_0$  and  $\sigma_8$  tensions, as discussed in the following. From Table 3.3, one can see that with the base data set: CMB + BAO,  $H_0 = 67.4 \pm 3.9 \text{ km s}^{-1} \text{ Mpc}^{-1}$  at 68% CL, is consistent with the Planck measurement. However, with the inclusion

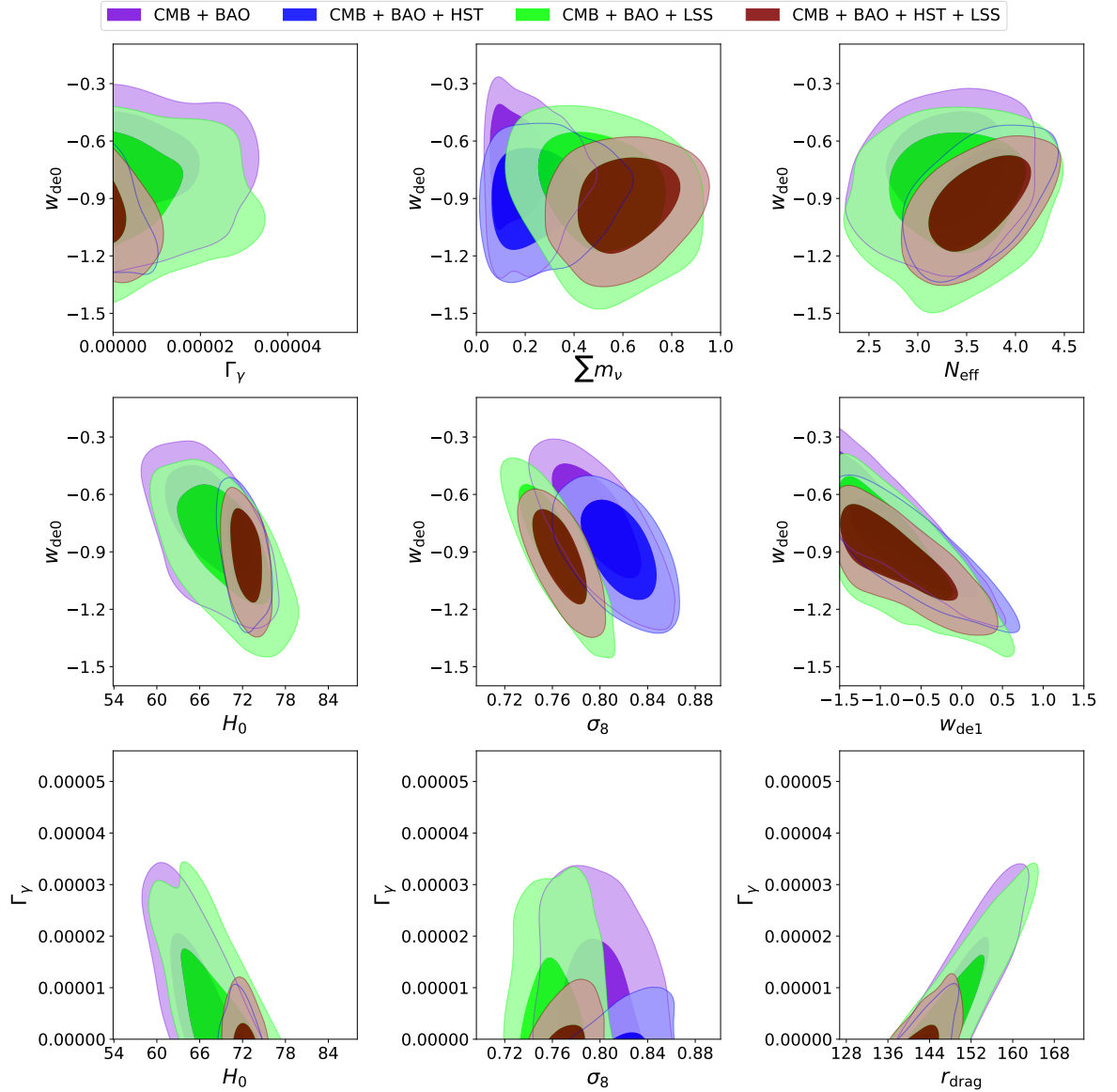


Figure 3.11: 68% and 95% confidence contours for some selected model parameters of DM-photon coupling model with variable DE.

of HST and LSS data to the base data, we have  $H_0 = 72.2 \pm 1.6 \text{ Km s}^{-1} \text{ Mpc}^{-1}$  and  $H_0 = 69.8 \pm 4.1 \text{ Km s}^{-1} \text{ Mpc}^{-1}$ , both at 68% CL, respectively. In the joint analysis, we obtain  $H_0 = 72.5 \pm 1.5 \text{ Km s}^{-1} \text{ Mpc}^{-1}$  at 68% CL. Thus, addition of HST and LSS data yields larger values of  $H_0$ , in line with the local value,  $H_0 = 73.24 \pm 1.74 \text{ Km s}^{-1} \text{ Mpc}^{-1}$  as reported by Riess *et al.* [39]. In the present analysis, we have obtained lower mean values on  $H_0$  in all the four cases as compared to our first case but still consistent with

the local measurement at 68% CL (see Figure 3.10). With regard to  $\sigma_8$  tension, one can note from the Table 3.3 that we have obtained lower values with  $\sigma_8 = 0.799_{-0.026}^{+0.020}$ ,  $\sigma_8 = 0.761_{-0.021}^{+0.017}$ , and  $\sigma_8 = 0.767_{-0.016}^{+0.014}$ , all at 68% CL from CMB + BAO, CMB + BAO + LSS and the joint analysis, respectively. These values are in good agreement with the direct measurements like galaxy cluster count, weak gravitational lensing and SZ cluster abundance measurements, etc. However, with the case CMB + BAO + HST, we have  $\sigma_8 = 0.816_{-0.020}^{+0.022}$  at 68% CL, favouring Planck CMB measurement. We observe that variable EoS of DE provides slightly lower values of  $\sigma_8$  with all data combinations as compared to our results in the previous model. In particular, a significant change is observed with the data combinations: CMB + BAO and CMB + BAO + LSS. One may see the consistency of the range of  $\sigma_8$  values, with the Planck-SZ measurement  $\sigma_8 = 0.75 \pm 0.03$  [43] in the right panel of Figure 3.10. Further, one may see the correlation of present DE EoS parameter  $w_{\text{de}0}$  and DM-photon coupling parameter  $\Gamma_\gamma$  with some other model parameters in Figure 3.11. In particular, we observe that  $w_{\text{de}0}$  shows a negative correlation with  $\sigma_8$  and  $H_0$  parameters with all data combinations. Thus, higher values of  $w_{\text{de}0}$  correspond to lower values of  $\sigma_8$ . In general, we notice that  $w_{\text{de}0}$  and  $\Gamma_\gamma$  show correlation with all other parameters especially in case of the full data combination. Next, we have found the upper bound on the neutrino mass scale as  $\sum m_\nu < 0.89$  eV at 95% CL with joint analysis: CMB + BAO + HST + LSS. We notice that the constraints on neutrino mass scale are similar to those obtained in our first study, with all data combinations. Also, one can see from Figure 3.11 that  $w_{\text{de}0}$  does not exhibit correlation with neutrino mass scale  $\sum m_\nu$ . Thus, we observe that time-varying DE does not have any significant effect on the neutrino mass scale. Next, in comparison to our previous model, here we have found significantly lower values  $N_{\text{eff}} = 3.29 \pm 0.39$  and  $N_{\text{eff}} = 3.40 \pm 0.40$ , both at 68% CL with CMB + BAO and CMB + BAO + LSS, respectively. The constraints on  $N_{\text{eff}}$  with other two data combinations are consistent with our first case. We have obtained constraints on  $r_{\text{drag}}$  similar to our first study. In Figure 3.11, one can see a positive correlation between  $\Gamma_\gamma$  and  $r_{\text{drag}}$ . The constraints on  $r_{\text{drag}}$  are in good agreement with the recent measures in [147, 148] at 68% CL.

Table 3.4: Difference of AIC values of considered models with respect to minimal  $\Lambda$ CDM model from all data combinations.

Data	$\Delta\text{AIC}_{\text{model1}}$	$\Delta\text{AIC}_{\text{model2}}$
CMB + BAO	9.88	9.56
CMB + BAO + HST	2.82	7.36
CMB + BAO + LSS	-0.08	-1.34
CMB + BAO + HST + LSS	-3.68	-4.80

### 3.5 Bayesian model comparison

In this section, we perform a statistical comparison of both the investigated models with a known well-fitted reference model (we have chosen the  $\Lambda$ CDM model). For this purpose, we use classical statistical criterion, namely, the AIC as discussed in subsection 2.1.4 of Chapter 2. Table 3.4 summarizes the difference of AIC values, i.e.,  $\Delta\text{AIC}$  of both the models with respect to the standard  $\Lambda$ CDM model for all data combinations. In case of model1, on the basis of AIC difference, the preference of  $\Lambda$ CDM model is only observed with the CMB + BAO data combination. For model2, we have found that  $\Delta\text{AIC}$  value is greater than the threshold value for the data combinations: CMB + BAO and CMB + BAO + HST. Therefore, it can be claimed that the standard  $\Lambda$ CDM model is strongly favored over the model2 with these two data combinations. For the other combinations, we can not claim statistical evidence in favor or against the  $\Lambda$ CDM model with respect to both the models, on the basis of AIC difference since  $\Delta\text{AIC}$  is less than the threshold value.

### 3.6 Concluding remarks

In this chapter, we have investigated two extensions of the  $\Lambda$ CDM model where a non-minimal DM-photon coupling is assumed. In the first case, the DE is characterized by constant EoS parameter whereas in the second case the time-varying DE EoS parameter is assumed. In both analyses, the massive neutrinos are also considered. We have observed significant effects of the considered cosmological scenario on the CMB TT and matter power spectra. We have obtained observational constraints on the DM-photon coupling

model parameters using the latest data from CMB, BAO, HST, and LSS. In the first case, we have found the upper bound on the coupling parameter, viz.,  $\Gamma_\gamma \leq 1.3 \times 10^{-5}$  using the full data set CMB + BAO + HST + LSS. As a direct consequence of the decay of DM into photons, we have found that this scenario can naturally solve the current tension on the Hubble constant by providing high values of  $H_0$  consistent with the local measurements. Thus, the cosmological model with DM-photon coupling has proved to be able to resolve the tension on  $H_0$ . In the second case, we have observed significant changes due to the time-varying EoS of DE on various model parameters. We have found that the mean value of  $w_{\text{de}0}$  favors quintessence behavior ( $w_{\text{de}0} > -1$ ) of DE with all data combinations (see left panel of Figure. 3.9). We have observed significant correlations of the DE EoS parameter  $w_{\text{de}0}$  with other model parameters (see Figure 3.11). Due to the decay of DM into photons, we have obtained higher values of  $H_0$ , consistent with the local measurements, similar to our first study. It is important to mention that the time-varying DE leads to lower values of  $\sigma_8$  in the DM-photon coupling model with all data combinations, in comparison to our first study. Thus, allowing time-varying DE in the DM-photon coupling scenario is useful to alleviate the  $H_0$  and  $\sigma_8$  tensions (see Figure 3.10). Therefore, an alteration in the standard dynamics of photons through the cosmic expansion can be a viable alternative to describe physics beyond the  $\Lambda$ CDM model in light of the current observational tensions.